Geofísica Internacional 47 (2), 115-126 (2008)

Transient response and multiple scattering of elastic waves by a linear array of regularly distributed cylindrical obstacles: Anti-plane S-wave analytical solution

R. Ávila-Carrera[1]*, F. J. Sánchez-Sesma[2] and J. Avilés[3]
[1]Instituto Mexicano del Petróleo, Mexico, City, Mexico.
[2]Instituto de Ingeniería, Universidad Nacional Autónoma de México. Mexico City, Mexico.
[3]Instituto Mexicano de Tecnología del Agua Jiutepec, Morelos. México.

Received: December 14, 2007; accepted: January 22, 2008

Resumen

Estudiamos la difracción múltiple de ondas elásticas por un arreglo lineal finito de obstáculos cilíndricos distribuidos regularmente. En particular, se resuelve con detalle la respuesta transitoria del sistema para la incidencia de ondas de corte antiplanas. Presentamos una extensión de la solución original para cilindros rígidos desarrollada por algunos de nosotros en los ochentas. La solución se obtiene formalmente para una excitación armónica en el dominio de la frecuencia y el análisis de Fourier nos permite obtener la respuesta transitoria. En este análisis mejorado se consideran variaciones en las propiedades de los materiales de las inclusiones cilíndricas. La formulación es bidimensional y se construye a partir de la superposición del campo incidente y las ondas difractadas por cada obstáculo. Las soluciones para cada obstáculo se construyen como expansiones de funciones de onda cilíndricas. La solución exacta se obtiene formalmente después de imponer condiciones de continuidad para los desplazamientos y las tracciones en las interfaces matriz-difractor con la ayuda del teorema de adición de Graf. Así, el campo total se puede referir a cualquier sistema de coordenadas cilíndrico. El sistema de ecuaciones infinito se aproxima por uno finito y esto permite obtener resultados numéricos para diferentes valores de los parámetros. Se estudian varios casos de cavidades e inclusiones. Se muestra que un doble efecto es producido por la presencia de un material particular de relleno: amplificaciones en el lado de la incidencia y reducciones en el lado opuesto, o vice versa. Se calculan también sismogramas sintéticos e instantáneas de tiempo con el objeto de ilustrar las características complejas de la propagación de ondas en este modelo inhomogéneo.

Palabras clave: Difracción múltiple, respuesta transitoria, solución analítica, ondas elásticas, obstáculos cilíndricos, instantáneas de tiempo.

Abstract

We study the multiple scattering of elastic waves by a finite linear array of regularly distributed cylindrical obstacles. The transient response of the system for incident anti-plane shear waves is given in detail. We present an extension of an original solution for rigid cylinders, developed by some of us in 1983. The solution is formally obtained for harmonic excitation and Fourier analysis provides the transient response. Material properties of the cylindrical inclusions are considered. A 2-D formulation is constructed by superposition of the incident field upon the waves diffracted by each obstacle. The solutions for each obstacle are constructed as expansions of cylindrical wave functions, after imposing continuity conditions for the displacements and tractions at the scatterers matrix interfaces with the aid of Graf's addition theorem. Thus, the total field can be referred to any cylindrical coordinates. The infinite system is approximated by a finite one and numerical results are obtained for different values of the parameters. Various cases of cavities and inclusions are studied. A double effect is produced by different filling materials, f. e. amplification at the incidence side and reductions at the far side, or *vice versa*. Synthetic seismograms and snapshots are computed to illustrate the complex features of wave propagation for this inhomogeneous model.

Key words: Multiple scattering, transient response, analytical solution, elastic waves, cylindrical obstacles, snapshots.

Introduction

Mathematical and numerical modeling is fundamental in science and engineering. In particular, geophysical modeling is crucial to understand basic features of hydrocarbon reservoirs in the field. Analytical formulations has allowed establishing benchmark solutions for some problems. Most of these formulations have been employed, among other uses; (1) to build basic solutions for more complicated problems, (2) for validation and calibration of new results and (3) for trustworthy field data interpretation. In scattering problems exact solutions have been helpful even thoung only some types of obstacles (i.e. cylinders, spheres or ellipsoids) yield exact analytical solutions. The insight gained by such applications is significant and useful.

Multiple scattering of elastic waves by a set of flexible inclusions was treated by Foldy (1945) and Lax (1951) for scalar waves, and subsequently by other authors (e. g. Waterman and Truell, 1961; Frisch, 1968; Varadan *et. al.*, 1978; Varadan and Varadan, 1980; Kikuchi, 1981; Avilés and Sánchez-Sesma, 1983). Most recent publications deal with the subject in 3D, e. g., asymptotic solutions of the dispersion equations in the long and short-wavelength regimes (Kanaun *et. al.*, 2004), acoustic wave propagation by cylindrical shells (Veksler *et. al.*, 2000), and elastic wave scattering by spheres (Gritto *et. al.*, 1995; 1999; Ávila-Carrera and Sánchez-Sesma, 2006). Some 2-D analytical solutions of the time response of a single cavity are presented by Davis *et. al.*, (2001) and by Yin-Bin *et. al.*, (2000) for the viscoelastic case. The books by Tsang *et. al.*, (2000), Ishimaru (1997) and Sheng (1995) cover the subject in the frequency domain reasonably well, but they leave aside the analysis of the time response. On the other hand, numerical techniques such as finite-difference and finite-element methods face limitations regarding computer time and core required when dealing with realistic scattering problems, even with state-of-the-art-computers (Vlastos *et. al.*, 2003).

In a previous work (Avilés and Sánchez-Sesma, 1983) we faced limitations imposed by computational conditions at the time. Only frequency domain results were presented and the cylinders were assumed to be rigid. In this paper, we review the theoretical analysis developed in the early 80's for rigid cylinders and we extend it to solve the transient response of multiple scattering of anti-plane incoming S-waves by a linear array of cylindrical elastic inclusions and cavities. Our aim is to study multiple diffraction of elastic waves presumably generated by a distant seismic source. We assume that the displacement field of the anti-plane shear motion is in the same direction as the axes of the cylinders. In future work we will address more realistic cases, including perpendicular motion of the wave field with respect to the axes. We consider closed-form analytical solutions for diffracted and reflected fields produced by various types of cylinders (cavities, rigid or elastic inclusions). The solution is constructed in the frequency domain as a superposition of incident and diffracted fields by each obstacle. Continuity and equilibrium conditions are enforced at all scatterer-matrix interfaces with the aid of Graf's addition theorem. Thus, the total field may be referred to any cylindrical coordinate system, by uncoupling the odd and even parts of the solution. From results in the frequency domain, Fourier synthesis yields the transient response. Previous work (e.g., Benites *et. al.*, 1992), dealt with infinite periodic arrays, and this work was taken into consideration. In our case the array is finite, and the formulation using Graf´s addition theorem leads to exact expressions so that edge effects are naturally included, but infinite wave expansions must be truncated to a practical size. In our examples, the order of wave expansions is commonly limited to ten or twelve which movides enough resolution for the studied configurations. Several examples of array configurations are shown. Normalized amplitudes of the displacement field *versus* distance for a given frequency are depicted. In order to illustrate the complex behavior of wave motion in this inhomogeneous model, synthetic seismograms and snapshots are computed. The results provide insight of multiple scattering behavior, and provide a quantitative description of various types of material fillers that can be used as references for calibration of other modeling techniques.

Formulation of the Problem

Consider a linear, elastic, isotropic and homogeneous space and let anti-plane displacement w be defined in the z direction. Consider a regular array of elastic cylinders with properties different from those of the surrounding material, as in Fig. 1. The propagation of harmonic plane S-waves satisfies the reduced wave equation, or Helmholtz equation

$$\frac{\partial^2 w}{\partial x^2} + \frac{\partial^2 w}{\partial y^2} + k^2 w = 0, \qquad (1)$$

where x, y = Cartesian coordinates, $k = \omega/\beta$ = shear wave-number, ω = angular frequency and $\beta = \sqrt{\mu/\rho}$ = shear wave propagation velocity; μ = shear modulus and ρ = mass density of the elastic space.

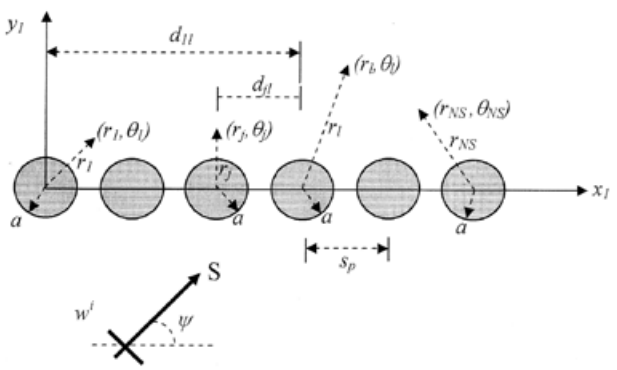

Fig. 1. Everly distributed array of elastic cylinders, system of reference and incoming anti-plane S-wave.

The excitation consists of a plane wave of amplitude w_0 with angle of incidence ψ, propagating in the forward direction toward the array of cylindrical inclusions, as shown in Fig. 1. This incident wave is expressed in the reference system (x_1, y_1) with respect to the first obstacle by

$$w^i(x_1, y_1) = w_0 \exp[-ik(x_1 \cos\psi + y_1 \sin\psi)]\exp(i\omega t). \quad (2)$$

The factor $\exp(i\omega t)$ ($i = \sqrt{-1}$ and t = time) for the time dependency of harmonic motion will be omitted from here on. The array of aligned cylinders produces diffraction and scattering of the incoming wave field. Thus, the solution can be represented by

$$w = w^i(x_1, y_1) + \sum_{j=1}^{NS} = w_j^s(r_j, \theta_j), \quad (3)$$

where $w_j^s(r_j, \theta_j)$ denotes the diffracted waves by the j-th cylinder as referred to its own coordinate system (r_j, θ_j), and NS = number of scatterers.

By separation of variables, the diffracted field for each scatterer can be written (Abramowitz and Stegun, 1964)

$$w_j^s(r_j, \theta_j) = \sum_{n=0}^{\infty} A_n^j H_n^{(2)}(kr_j)\cos n\theta_j + \sum_{n=0}^{\infty} B_n^j H_n^{(2)}(kr_j)\sin n\theta_j, \quad (4)$$

where A_n^j, B_n^j = unknown complex coefficients that will be determined from the boundary conditions, and $H_n^{(2)}(\cdot)$ = Hankel function of the second kind and order n. The wave functions $H_n^{(2)}(kr_j)\cos n\theta_j$ and $H_n^{(2)}(kr_j)\sin n\theta_j$ represent a complete set of solutions of the reduced wave equation in unbounded regions which satisfy the Sommerfeld radiation condition (Mow and Pao, 1971). When we have elastic obstructions, part of the incident wave field is refracted and a stationary wave is generated inside each cylinder. By solving (1), the refracted field in the j-th cylinder can be expressed in the local coordinate system (r_j, θ_j) as

$$w_j(r_j, \theta_j) = \sum_{n=0}^{\infty} C_n^j J_n(k_c r_j)\cos n\theta_j + \sum_{n=0}^{\infty} D_n^j J_n(k_c r_j)\sin n\theta_j, \quad (5)$$

where C_n^j, J_n = unknown complex coefficients that will be determined from the boundary conditions, and $J_n(\cdot)$ = Bessel function of the first kind and order n; the subscript c of the wave number k_c refers to cylinder. The functions $J_n(k_c r_j)\cos n\theta_j$ and $J_n(k_c r_j)\sin n\theta_j$ represent a complete set of solutions of the reduced wave equation in bounded regions. All coefficients A_n^j, B_n^j, C_n^j and D_n^j that define the solution of the problem are obtained when the boundary conditions are fulfilled.

Let us assume perfect contact between the cylinders and the surrounding elastic material, so that the boundary conditions at the matrix-obstruction interfaces are continuity of displacements and stresses:

$$w(r_l, \theta_l)\big|_{r_l=a} = w_l(r_l, \theta_l)\big|_{r_l=a} \quad 0 \le \theta_l \le 2\pi \text{ and } l = 1, 2, \ldots \text{NS}, \quad (6)$$

$$\mu \frac{\partial w(r_l, \theta_l)}{\partial r_l}\bigg|_{r_l=a} = \mu_c \frac{\partial w_l(r_l, \theta_l)}{\partial r_l}\bigg|_{r_l=a} \quad 0 \le \theta_l \le 2\pi \text{ and } l = 1, 2, \ldots \text{NS}, \quad (7)$$

where a = radius of the cylinders. Salving the problem requires imposing the boundary conditions at each cylinder. For convenience, the total field in (3) will be given with respect to the arbitrary coordinate system (r_l, θ_l). Eqs. (2) and (4) must be referred to this coordinate system using Graf's addition theorem (see Appendix). This the total field becomes

$$\begin{aligned} w(r_l, \theta_l) = w_0 \Bigg[& \sum_{m=0}^{\infty} \varepsilon_m (-1)^m \cos m\psi J_m(kr_l)\cos m\theta_l + \\ & 2\sum_{m=1}^{\infty} (-i)^m \sin m\psi J_m(kr_l)\sin m\theta_l \Bigg] + \\ (1-\delta_{l1}) \sum_{j=1}^{l-1} \Bigg[& \sum_{n=0}^{\infty} A_n^j \sum_{m=0}^{\infty} (-1)^m \frac{\varepsilon_m}{2} K_m^n(kd_{jl}) J_m(kr_l)\cos m\theta_l + \\ & \sum_{n=1}^{\infty} B_n^j \sum_{m=1}^{\infty} (-1)^m L_m^n(kd_{jl}) J_m(kr_l)\sin m\theta_l \Bigg] + \\ & \sum_{m=0}^{\infty} A_m^l H_m^{(2)}(kr_l)\cos m\theta_l + \sum_{m=1}^{\infty} B_m^l H_m^{(2)}(kr_l)\sin m\theta_l + \\ (1-\delta_{lNS}) \sum_{j=l+1}^{NS} \Bigg[& \sum_{n=0}^{\infty} (-1)^n A_n^j \sum_{m=0}^{\infty} \frac{\varepsilon_m}{2} K_m^n(kd_{jl}) J_m(kr_l)\cos m\theta_l + \\ & \sum_{n=1}^{\infty} (-1)^n B_n^j \sum_{m=1}^{\infty} L_m^n(kd_{jl}) J_m(kr_l)\sin m\theta_l \Bigg] \end{aligned} \quad (8)$$

where

$$K_m^n(\cdot) = H_{n+m}^{(2)}(\cdot) + (-1)^m H_{n-m}^{(2)}(\cdot) \quad (9)$$

$$L_m^n(\cdot) = H_{n+m}^{(2)}(\cdot) + (-1)^m H_{n-m}^{(2)}(\cdot) \quad (10)$$

in which ε_m = Neumann factor ($\varepsilon_0 = 1$ and $\varepsilon_m = 2$, $m \ge 1$), d_{jl} = distance between the centers of the j-th and the l-th cylinders and δ_{lj} = Kronecker delta (= 1 if $l = j$; = 0 if $l \ne j$).

Inserting (5) and (8) into (6) and (7), and making use of the orthogonal properties of trigonometric functions, we obtain four infinite systems of algebraic equations for the coefficients A_n^j, B_n^j, C_n^j and D_n^j. However, we are interested in the solution for elastic media only, so the coefficients C_n^j and D_n^j can be eliminated and the four equation systems are reduced to two in follows

$$\begin{aligned} & (1-\delta_{l1})(-1)^m \sum_{j=1}^{l-1} \sum_{n=0}^{\infty} K_m^n(kd_{jl}) A_n^j + \frac{2}{\varepsilon_m} \left[\frac{H_m^{(2)'}(ka) - F_m H_m^{(2)}(ka)}{J'_m(ka) - F_m J_m(ka)} \right] A_m^l + \\ & (1-\delta_{lNS}) \sum_{j=l+1}^{NS} \sum_{n=0}^{\infty} (-1)^n K_m^n(kd_{jl}) A_n^j \end{aligned} \quad (11)$$

$$-2w_0(-i)^m \cos m\psi, \; l = 1, 2\ldots, NS \text{ and } m = 0, 1\ldots, \infty$$

$$\begin{aligned} & (1-\delta_{l1})(-1)^m \sum_{j=1}^{l-1} \sum_{n=0}^{\infty} L_m^n(kd_{jl}) B_n^j + \left[\frac{H_m^{2)'}(ka) - F_m H_m^{(2)}(ka)}{J'_m(ka) - F_m J_m(ka)} \right] B_m^l + \\ & (1-\delta_{lNS}) \sum_{j=l+1}^{NS} \sum_{n=0}^{\infty} (-1)^n L_m^n(kd_{jl}) B_n^j \end{aligned} \quad (12)$$

$$-2w_0(-i)^m \sin m\psi, \; l = 1, 2\ldots, NS \text{ and } m = 1\ldots, \infty$$

where

$$Fm = \sqrt{\frac{\mu_c \rho_c}{\mu \rho}} \frac{J_m'(k_c a)}{J_m(k_c a)}, \qquad (13)$$

in which the prime denotes differentiation with respect to the argument.

Notice that the azimuthal decomposition of the solution (8), reduces the triple summation to a double one, using the linear independence of the azimuthal functions cos $n\theta_j$ and sin $n\theta_j$. This boundary conditions (6) and (7) are imposed at every cylinder l for each azimuthal number *m*. Similar equations arise for the fields whitin each cylinder. As they are simpler, the constants can be eliminated substituted and the influence of the cylinders can be lumped together in the diagonal. Solving the systems of equations (11) and (12) completes the solution. However, such systems can not be solved exactly. An approximation is obtained by reducing the dimensions of equations to a finite number, by truncating the orders of expansions (*m* and *n*) such that the solution converges. By inspection of the systems of equations, it is found that the type of scatterer (elastic, rigid or cavity) modifies only the diagonal coefficients.

Numerical Results

In this section we show some relevant results obtained by the analytical technique described above. The aim is to present instructive examples in a simple way. Configurations for each model analyzed are depicted and the ensuing results are discussed. Eight to ten terms were used for the wave expansions, obtaining up to four-digit accuracy in the range of frequencies studied. Normal and oblique incidence of plane waves were considered for all cases presented. The wave field depends on the nondimensional frequency given by

$$\eta_k = \frac{ka}{\pi} = \frac{2a}{\lambda_k}, \qquad (14)$$

where λ_k = wavelength of the incident S-wave. Thus, the normalized frequency represents the diameter of the cylinder over the wavelength.

In Fig. 2 the normalized displacement amplitude with respect to the free-field displacement for an array of eight scatterers has been calculated. Displacement is plotted against distance *x*/*a* along the array axis. Four cases are analyzed in terms of separation between cylinders and distance *y*/*a* at the far side of incidence. Three kinds of material fillers have been considered: short dashed lines correspond to elastic cylinders with $\rho_c/\rho = 0.5$ and $\mu_c/\mu = 0.3$, long dashed lines to cavities with $\rho_c/\rho = 0$ and $\mu_c/\mu = 0$, and solid lines to rigid cylinders with $\rho_c/\rho = 1.538$ and $\mu_c \to \infty$. Dimensionless frequency $\eta_k = 0.5$ and normal incidence of wave excitation have been used for the computations. It is remarkable that, for a given frequency, the amplitude of the displacement field suffer a strong attenuation when an array of rigid cylinders is used. The results for cavities and elastic cylinders are quite similar; they appear to be sensitive to changes in separation between obstacles.

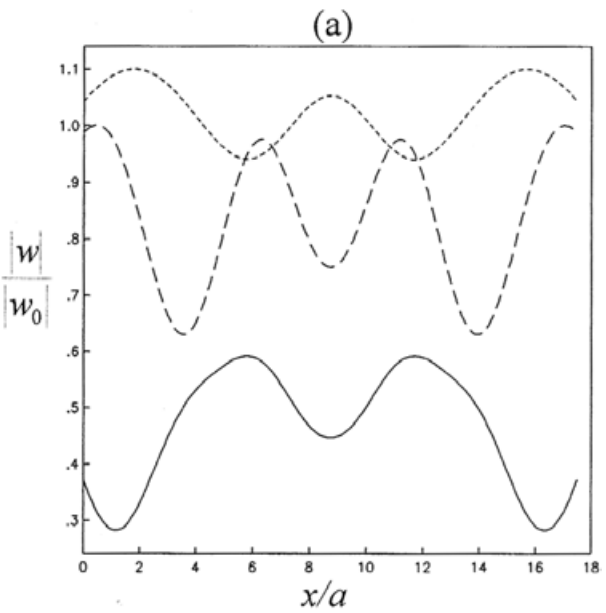

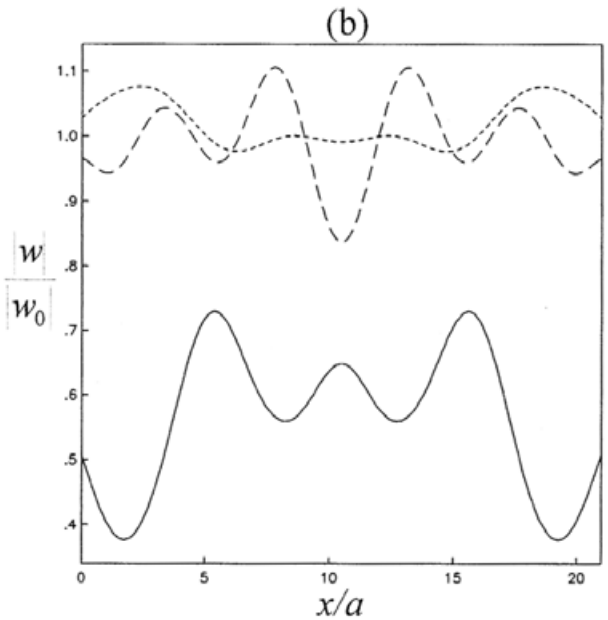

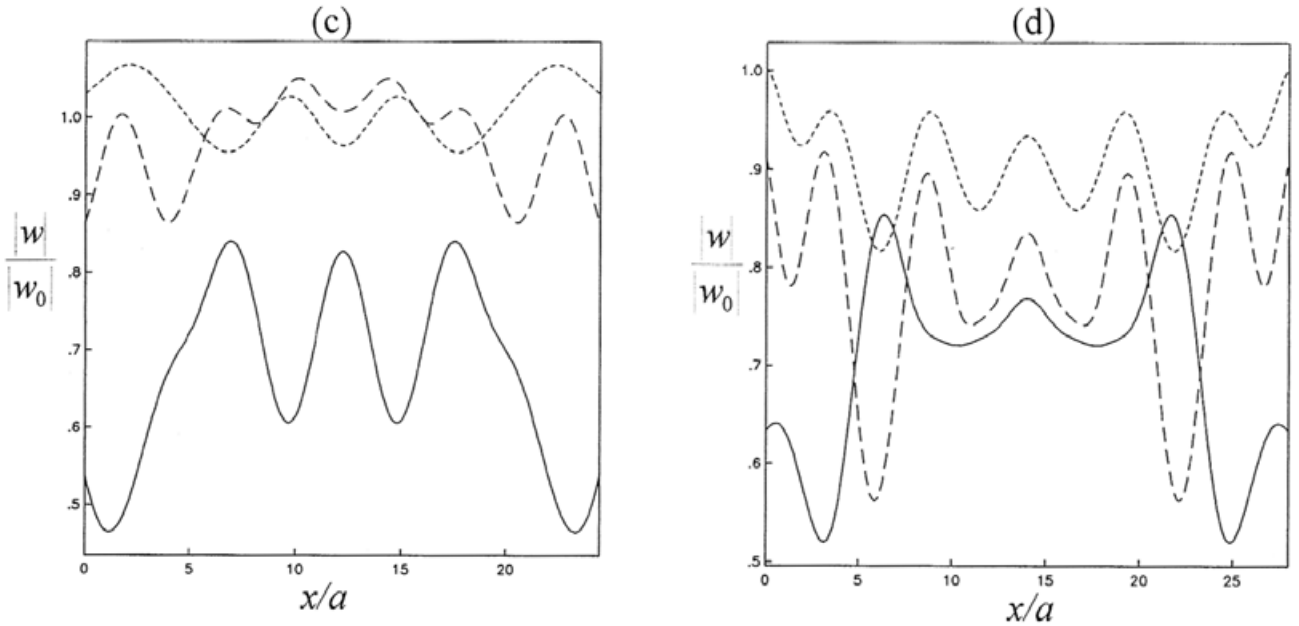

Fig. 2. Normalized displacement amplitudes for the model of Fig. 1 with $NS = 8$. Several distances y/a and various separations between cylinders s_p/a. (a) $y/a = 8.75$, $s_p/a = 2.5$. (b) $y/a = 10.5$, $s_p/a = 3.0$. (c) $y/a = 12.25$, $s_p/a = 3.5$ and (d) $y/a = 14.0$, $s_p/a = 4.0$.

For a more detailed view of the sharp decrease in amplitude due to the presence of rigid scatterers as previously discussed by Avilés and Sánchez-Sesma (1983), it is convenient to compute the displacements at the far side of incidence in a relative distant field ($y/a = 150$). In Fig. 3, normalized amplitudes of the displacement field w/w_0 against distance x/a are shown. Separations between cylinders of $s_p/a = 2.5$, 3.0, 3.5 and 4.0, and a normalized frequency $\eta_k = 0.5$ under incidence of S-waves were taken for the computations. Maximum reductions occur near the center of the array. This effect is clearly appreciated in Fig. 3 for a normalized separation $s_p/a = 3$. In this case, the reductive effect of the system is of the order of 55%, and 60% for a separation of $s_p/a = 2.5$. Thus the system behaves like a single unit at long distances and not as a set of independent scatterers. From Figs. (2) and (3) it is clear

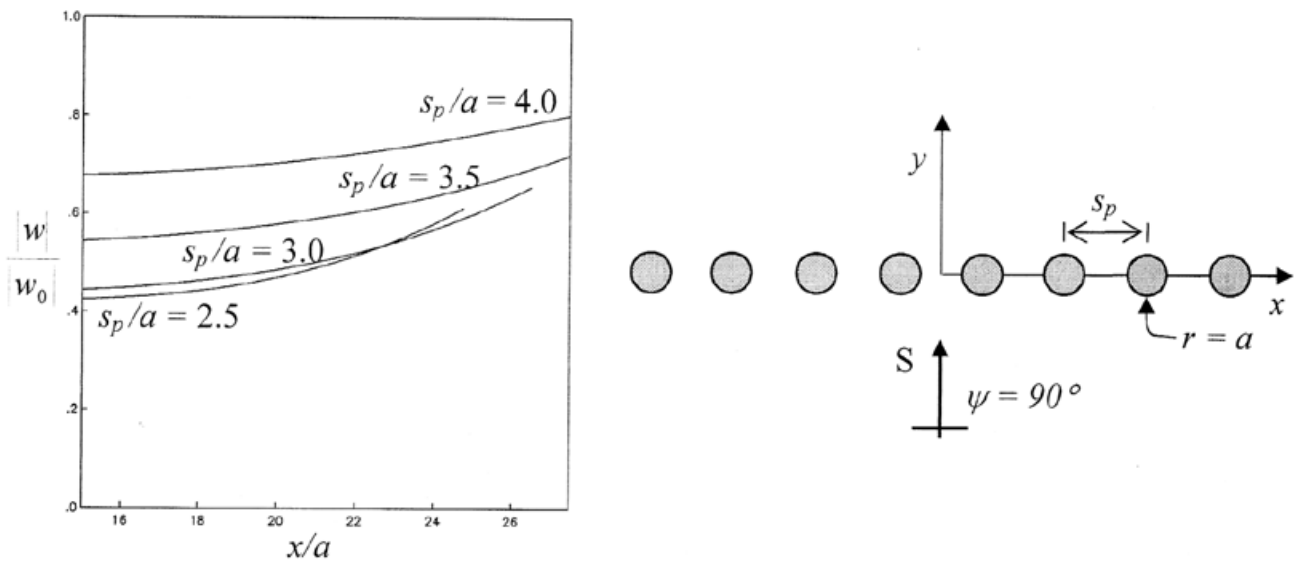

Fig. 3. Normalized displacement amplitudes on $y/a = 150$ for an array of $NS = 8$ rigid cylinders with $\rho_c/\rho = 1.538$ and $\mu_c \rightarrow \infty$. Different separations between obstacles s_p/a, and nondimensional frequency, $\eta_k = 0.5$. Incidence of anti-plane S-waves.

that at points near the array of rigid obstacles, the reduced field shows large variability, in contrast with the smooth variations observed at long distances. As expected, when the obstacles are spaced closely, whit a separation of at least one radius, the maximum amplitude reductions take place. As the separation increases reductions become less significant.

To show the scattering effects at the incidence side, normalized displacement amplitudes for an eight obstacle array have been calculated. Three kinds of material fillers (cavities, elastic inclusions and rigid cylinders) were considered. The distance between centers of scatterers is s_p/a = 4.0 and the nondimensional frequency is η_k = 0.4. Results for several distances at the incidence side (y/a = -5, -10, -15 and -20) are displayed in Fig. 4a for cavities with $\rho_c/\rho = 0$ and $\mu_c/\mu = 0$, in Fig. 3b for elastic inclusions with ρ_c/ρ = 0.5 and μ_c/μ = 0.3, and in Fig. 4c for rigid cylinders with ρ_c/ρ = 1.538 and $\mu_c \to \infty$. For the arrays with cavities and elastic inclusions, a smooth amplification occurs that tends to disappear when we get close to the edges. With rigid cylinders the amplification effect occurs everywhere and maximum amplitudes at x/a = 22.25 for y/a = -20.

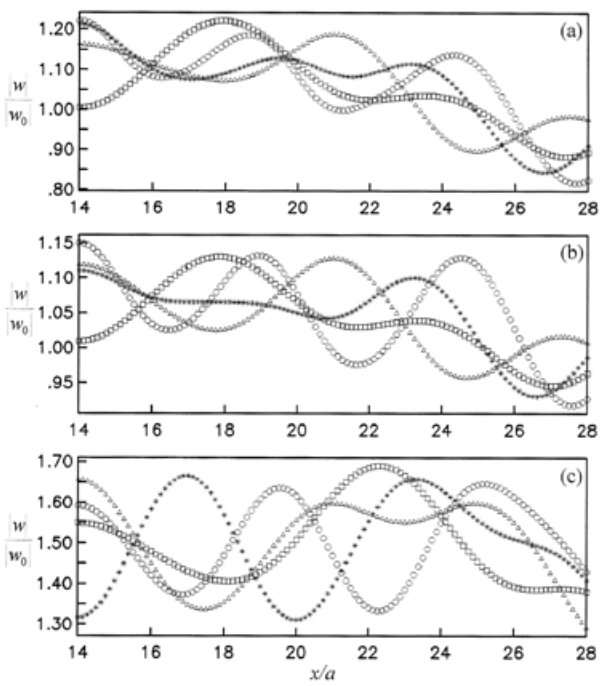

Fig. 4. Normalized displacement amplitudes for the model of Fig. 3 on several distances y/a = -20 (squares), y/a = -15 (triangles), y/a = -10 (asterisks), y/a = -5 (circles). Same properties as in Fig. 2 for (a) cavities, (b) elastic obstacles and (c) rigid obstacles. Incidence of anti-plane S-waves, nondimensional frequency $\eta_k = 0.4$.

So far, with the available set of results we observe a common double effect produced by several configurations of cylinders. Amplifications are generated at the incidence side and reductions take place at the far side. Fig. 5 shows the normalized amplitudes of the displacement field along x/a = 0, that is at the end of the array, for eight cylinders with separation s_p/a = 3.0 and dimensionless frequency η_k = 0.4. The short dashed line corresponds to an array of elastic cylinders with ρ_c/ρ = 0.5 and μ_c/μ = 0.3, long dashed line for cavities with ρ_c/ρ = 0.0 and μ_c/μ = 0.0, and solid line for rigid scatterers with ρ_c/ρ = 1.538 and $\mu_c \to \infty$. Notice the strong attenuation by the array for all three cases computed. The effect is strongest for rigid cylinders. The type of material filler seems ir relevant to amplitude reductions after the array. This fact must be checked by some time domain computations to follow.

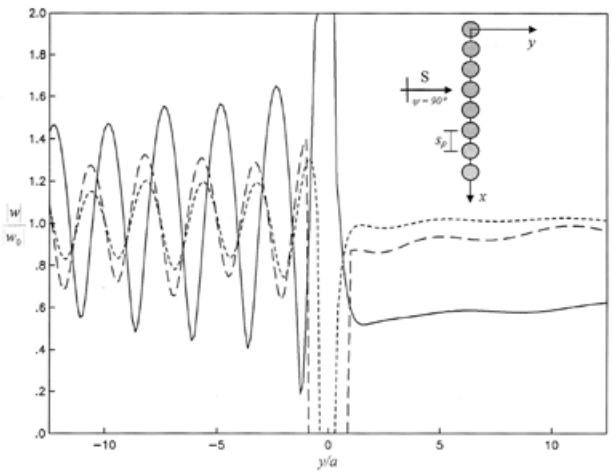

Fig. 5. Normalized displacement amplitudes on x/a = 0 for s_p/a = 3.0. Short dashed line corresponds to an array of elastic cylinders, long dashed line for cavities, and solid line for rigid scatterers. Incidence of anti-plane S-waves, nondimensional frequency, $\eta_k = 0.4$.

In order to show the characteristic time response of the studied models, several computations of time history in a fixed linear or spatial distribution of receivers were performed. Figs. 6 to 9 show the Fourier synthetic seismograms computed for models of two and four cylindrical scatterers. Normal and oblique incidences of S-waves were considered. Cavities, elastic inclusions and rigid cylinders were used in the computations. The seismometers are located at the far side of the array with respect to the incoming wave field. These configurations were adopted in order to observe forward scattering and the behavior of the propagating wave front due to the presence of the array.

Fig. 6 shows a simple model of two obstacles with radius $r = a = 1$ and separation between centers of $s_p/a =$ 4.0. There are 51 receivers at $x = \pm 4a$ and $z = 1.5$a; this configuration will be the same for all synthetic examples. The source is given by an S-wave field with an incidence angle of $\psi = 90^0$, the time variation is constructed a Ricker pulse with $t_p = 1.5$s and $t_p = 4$s. The elastic parameters are given by $\rho_c/\rho = 0.0$ and $\mu_c/\mu = 0.0$ for cavities (Fig. 6(a)), $\rho_c/\rho = 0.5$ and $\mu_c/\mu = 0.3$ for elastic cylinders (Fig. 6(b)), and $\rho_c/\rho = 1.538$ and $\mu_c \rightarrow \infty$ for rigid cylinders (Fig. 6(c)). Fig. 7 corresponds to the same model as in Fig. 6, except that the incidence angle is $\psi = 75^0$. Notice the arrival phases r_1, c_1, r_2, and c_2 produced by the interaction between the incident wave *d* and the obstacles *1* and *2* respectively. The letter *r* means *"reflecting"*, and the letter *c* means *"creeping"*, following the notation proposed by Benites *et. al.*, (1992). To observe the wave motion produced by the various configurations sketched here, note the 3rd generation arrival phases, i. e. r_{121} and r_{212}. These phases correspond to the reflected and creeping waves between the boundaries of the two scatterers, taking into account the order in which the reflection or creeping occurs. The indices are related to the order in which each interaction take place. For example, r_{21} indicates that the wave was reflected by scatterer *2* and next by scatterer *1*, before reaching receiver, in similar way for r_{121}. These phases are called *"interactive phases"* (Benites *et. al.*, 1992). Note that for the cases of cavities and elastic inclusions such phases are separated by time intervals of approximately $2a/\beta$. Normal S-wave incidence clearly shows how the incident field is delayed by the presence of the cavities. In the elastic examples, we observe a strong delayed amplification of the incident field due to the soft properties of obstacles. Creeping waves c_1 and c_2, are easily identified due to their higher amplitude relative to reflected phases r_1, r_2, and r_{21}. The traces for rigid obstacles reveal that creeping and reflecting phases follow the same wave paths.

Fig. 8 shows the same examples as in Fig. 6, except that for a four-scatterer array. Again, the response of three kinds of obstacles before an incoming plane S-wave field is depicted. Fig. 9 corresponds to the same parameter configuration as in Fig. 8, except for the case of $\psi = 75°$. In both figures, it is possible to identify the phases generated by the four scatterers, reflections r_3, r_4, r_{32}, r_{31}, r_4, r_{43}, r_{42} and r_{41}, Creeping phases c_3 and c_4 are also observed. While the wave paths appear to be regular, a graphic detail and longer duration is required to improve identification of 4th and 5th order phases. For cavities and elastic inclusions, the wave slopes follow similar propagation paths, but for rigid obstacles propagation suffers an interference effect between cylinders. With the four obstacle types we are able to generalize the wave motion and scattering patterns caused by any number of scatterers for linear arrays.

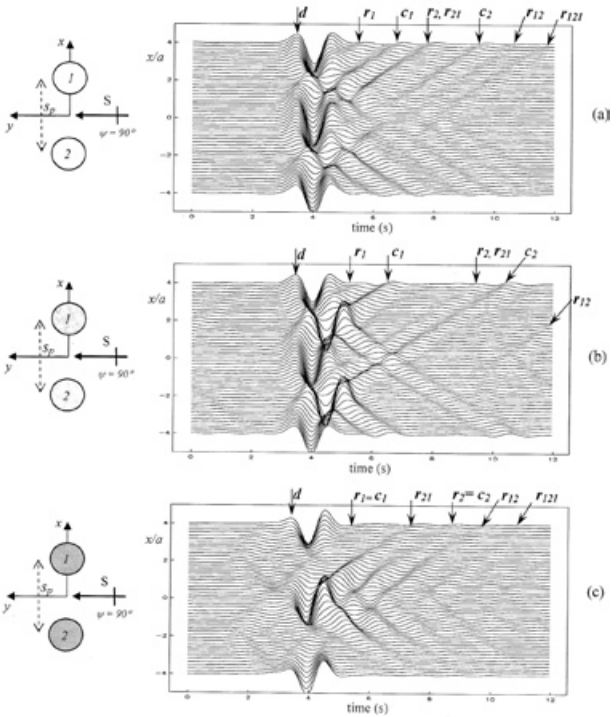

Fig. 6. Synthetic seismograms for the sketched models at left with *NS* = 2. Observation line of 51 receivers on *y/a* = 1.5 for various obstacles properties: (a) cavities, (b) elastic cylinders and (c) rigid cylinders. Excitation given by normal incidence of anti-plane S-waves and a Ricker wavelet.

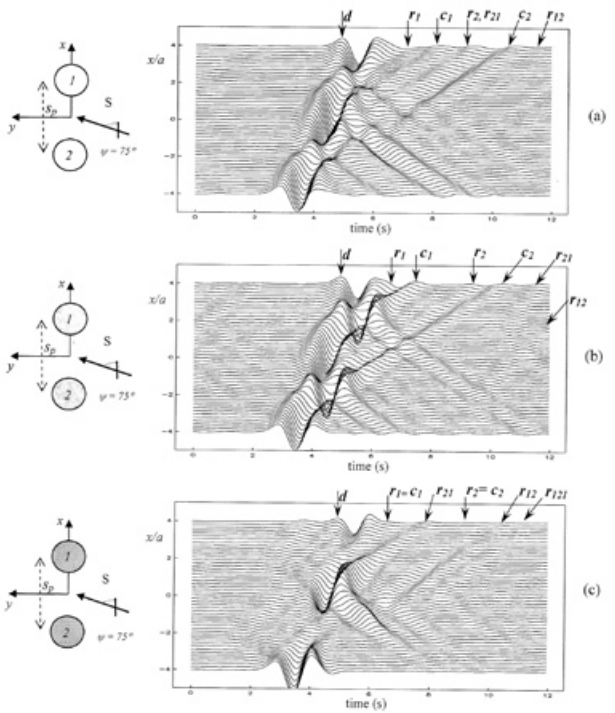

Fig. 7. Synthetic seismograms for the sketched models at left with *NS* = 2. Observation line of 51 receivers on *y/a* = 1.5 for various obstacles properties: (a) cavities, (b) elastic cylinders and (c) rigid cylinders. Excitation given by an oblique incidence of anti-plane S-waves and a Ricker wavelet.

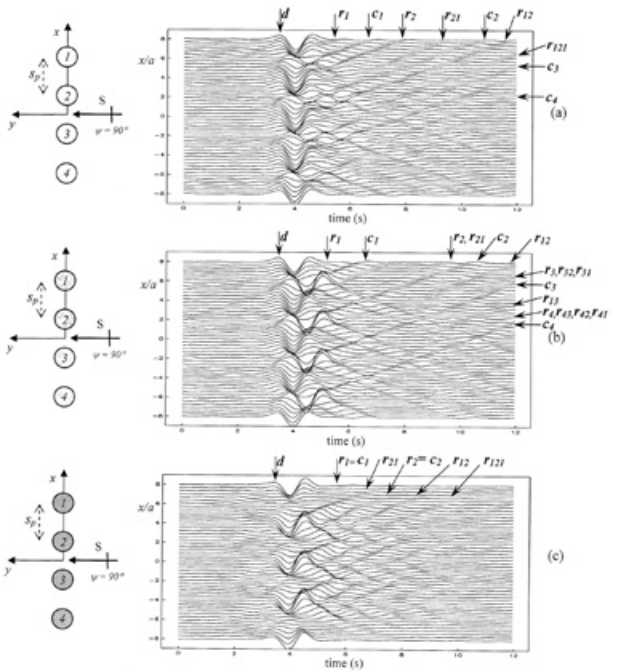

Fig. 8. Synthetic seismograms for the sketched models at left with *NS* = 4. Observation line of 51 receivers on *y*/*a* = 1.5 for various obstacles properties: (a) cavities, (b) elastic cylinders and (c) rigid cylinders. Excitation given by normal incidence of anti-plane S-waves and a Ricker wavelet.

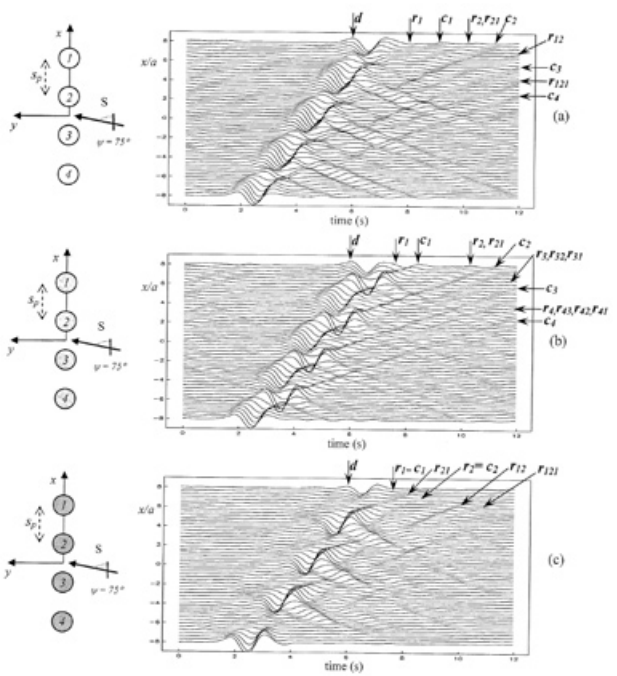

Fig. 9. Synthetic seismograms for the sketched models at left with *NS* = 4. Observation line of 51 receivers on *y*/*a* = 1.5 for various obstacles properties: (a) cavities, (b) elastic cylinders and (c) rigid cylinders. Excitation given by an oblique incidence of anti-plane S-waves and a Ricker wavelet.

Finally, consider wave motion and scattering patterns for the previously presented models. We have studied the spatial of amplitudes distribution during a lapse of propagation time, by means of snapshot series for meshes with 101 x 101 evenly spaced receivers located within squares of lengths 8*a* and 16*a*. In all cases twelve frames of displacement field are depicted. Figs. 10 and 11 show snapshots for a two cavity model ($\rho_c/\rho = 0.0$, $\mu_c/\mu = 0.0$) for $\psi = 90°$ and $\psi = 75°$ respectively. The centers of the cavities are located at $x = \pm 2$ and $y = 0$. The observation area is given by a square grid of receptors with length 8*a*. Excitation is given by anti-plane S-waves with a Ricker wavelet of $t_p = 0.8$s. Figs. 12 and 13 show a similar case for elastic cylinders ($\rho_c/\rho = 0.5$, $\mu_c/\mu = 0.3$). These set of results illustrate how the wavefront reaches the array and then reflections and diffractions are produced. Forward and backward scattering patterns are generated in the whole space. Delay and degeneration of wavefront by geometrical multiple diffraction from cavities is notorious. However, diffraction at the far side of incidence creates a shadow or gap due to the cavities, unlike elastic inclusions where an amplification effect is clearly seen. Results from elastic inclusions reveal that the wavefront is attenuated at reflecting phases and amplified at creeping phases, due to

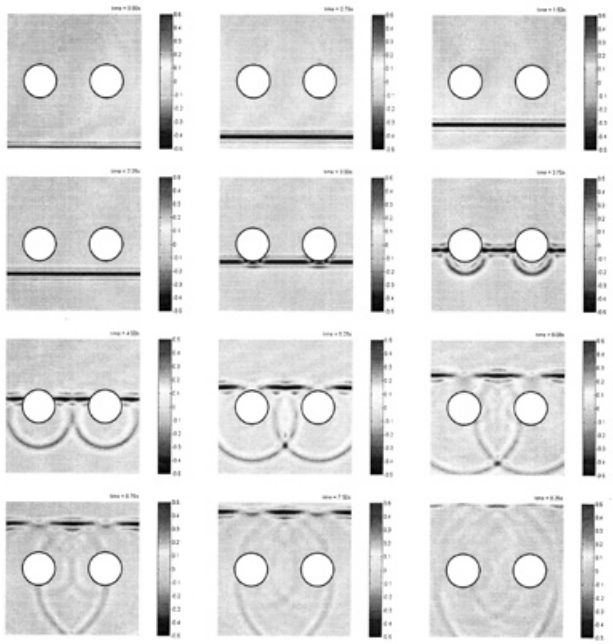

Fig.10. Snapshots of the displacement field for the model given in Fig. 6(a) (two cavities). Twelve times are depicted from $t_i = 0.0$s to $t_i = 8.25$s. The observation area is defined by $-4a \leq x \leq 4a$ and $-4a \leq y \leq 4a$. Excitation given by normal incidence of anti-plane S-wave and a Ricker wavelet of $t_p = 0.8$s.

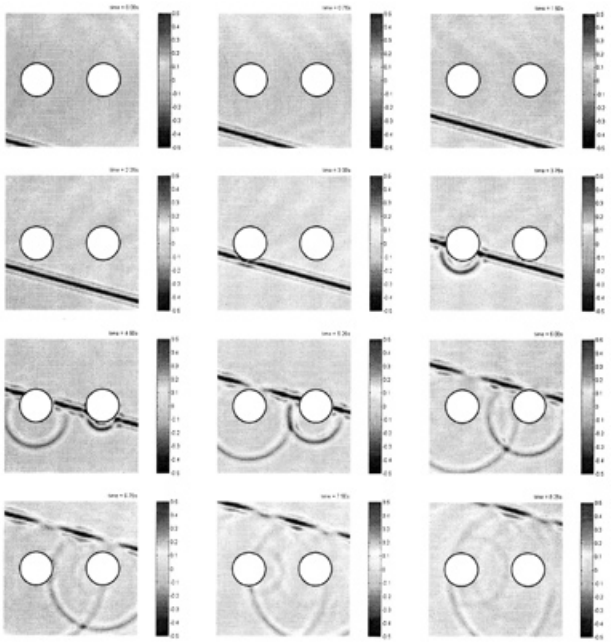

Fig.11. Snapshots of the displacement field for the model given in Fig. 7(a) (two cavities). Twelve times are depicted from t_i = 0.0s to t_i = 8.25s. The observation area is defined by -4a≤ x≤4a and -4a≤ y≤4a. Excitation given by oblique incidence of anti-plane S-wave $\psi = 75°$ and a Ricker wavelet of t_p = 0.8s.

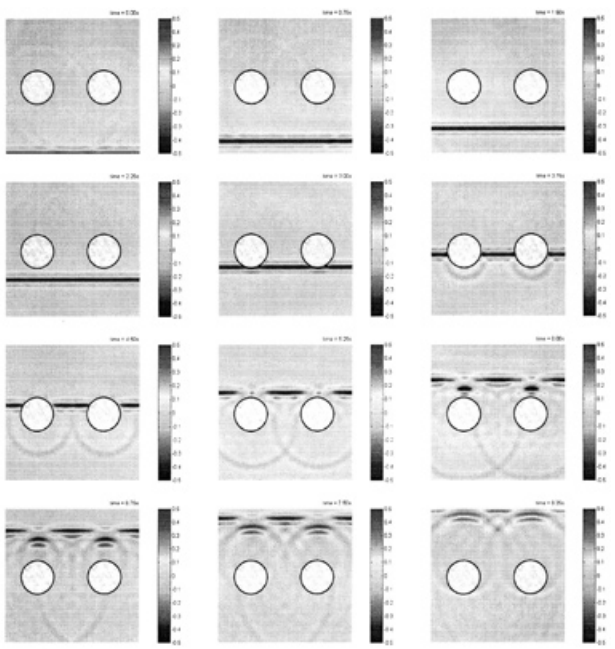

Fig.12 Snapshots of the displacement field for the model given in Fig. 6(b) (two elastic inclusions). Twelve times are depicted from t_i = 0.0s to t_i = 8.25s. The observation area is defined by -4a≤ x≤4a and -4a≤ y≤4a. Excitation given by normal incidence of anti-plane S-wave and a Ricker wavelet of t_p = 0.8s.

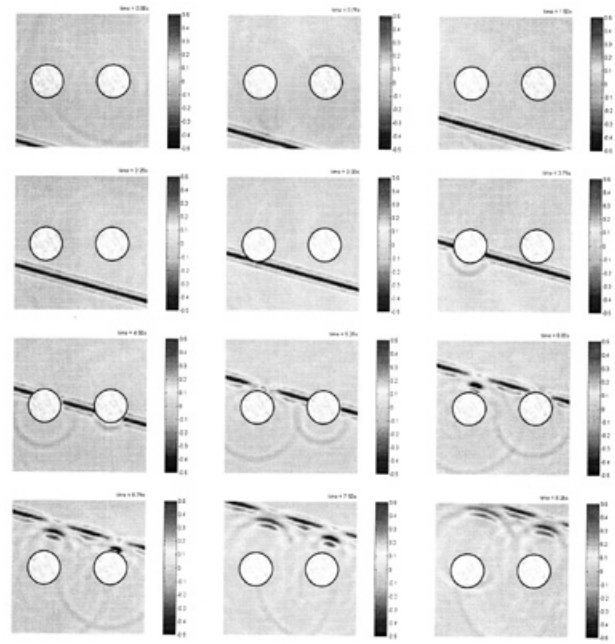

Fig.13. Snapshots of the displacement field for the model given in Fig. 7(b) (two elastic inclusions). Twelve times are depicted from t_i = 0.0s to t_i = 8.25s. The observation area is defined by -4a≤ x≤4a and -4a≤ y≤4a. Excitation given by oblique incidence of anti-plane S-wave $\psi = 75°$ and a Ricker wavelet of t_p = 0.8s.

the softer material filler. As time increases the wavefront recovers and the scattering of the wave field by the array wave diminishes. Again, it is possible to identify the interactive phases over the entire propagation space, but this exercise is left to the reader.

Figs. 14 and 15 show snapshots for a four cavity model with $\psi = 90°$ and $\psi = 75°$ respectively. The centers of the cavities are located at x = ±2 and x = ±6 with y = 0. The observation area is given by a square region of length 16a. Excitation is given by anti-plane S-waves with a Ricker wavelet of t_p = 1.0s. Figs. 16 and 17 show a similar previous case, just that for a four elastic inclusions model (ρ_c/ρ = 0.5, μ_c/μ = 0.3). The same responses described for the two cylinder models are recognized. The scattering patterns from the reflecting and creeping phases are dearly due to the higher number of regular obstacles in the array. Time analysis permits the observation of propagation properties that are not seen in the frequency domain, e. g. conspicuous amplification peaks produced by the diffraction of the wavefront due to softer elastic inclusions. Wave motion and scattering patterns produced by any number of cylinders in linear arrays may be characterized by the interaction between afew of them.

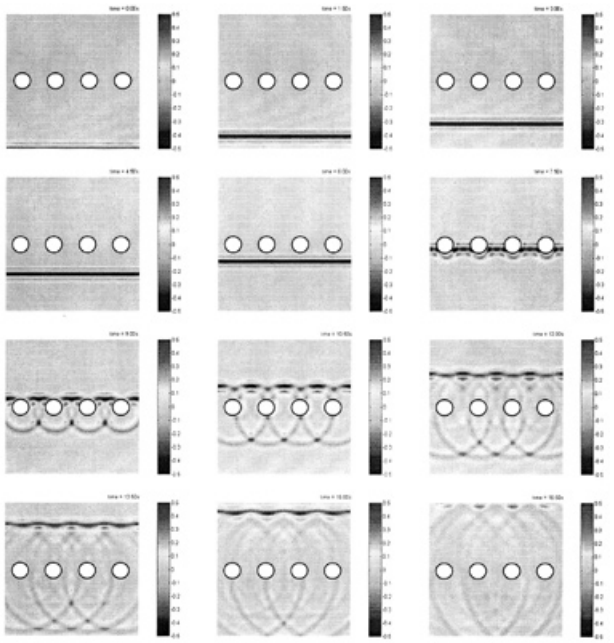

Fig.14. Snapshots of the displacement field for the model given in Fig. 8(a) (four cavities). Twelve times are depicted from t_i = 0.0s to t_i = 16.5s. The observation area is defined by -8a≤ x≤8a and -8a≤ y≤8a. Excitation given by normal incidence of anti-plane S-wave and a Ricker wavelet of t_p = 1.0s.

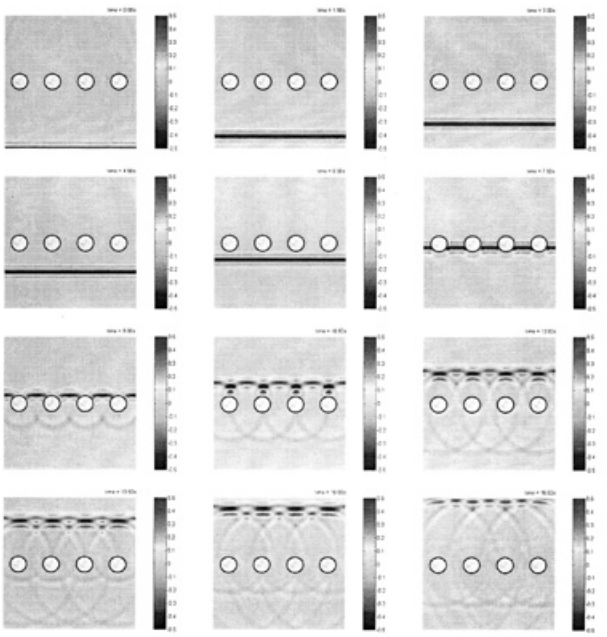

Fig.16. Snapshots of the displacement field for the model given in Fig. 8(b) (four elastic inclusions). Twelve times are depicted from t_i = 0.0s to t_i = 16.5s. The observation area is defined by -8a≤ x≤8a and -8a≤ y≤8a. Excitation given by normal incidence of anti-plane S-wave and a Ricker wavelet of t_p = 1.0s.

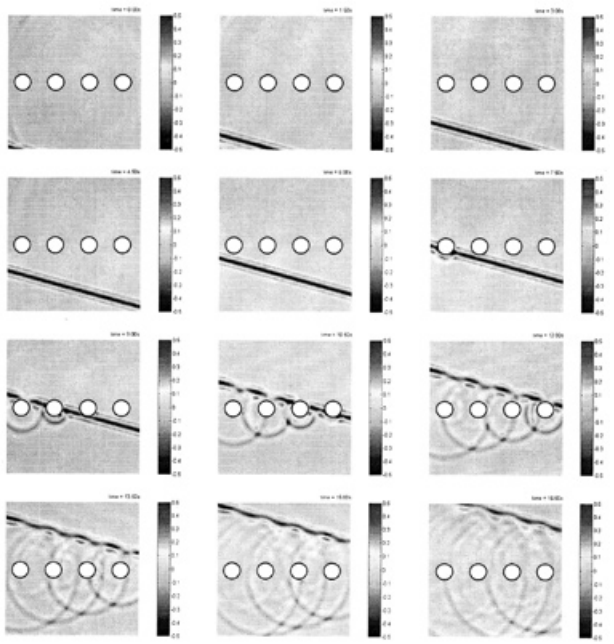

Fig.15. Snapshots of the displacement field for the model given in Fig. 9(a) (four cavities). Twelve times are depicted from t_i = 0.0s to t_i = 16.5s. The observation area is defined by -8a≤ x≤8a and -8a≤ y≤8a. Excitation given by oblique incidence of anti-plane S-wave ψ = 75° and a Ricker wavelet of t_p = 1.0s.

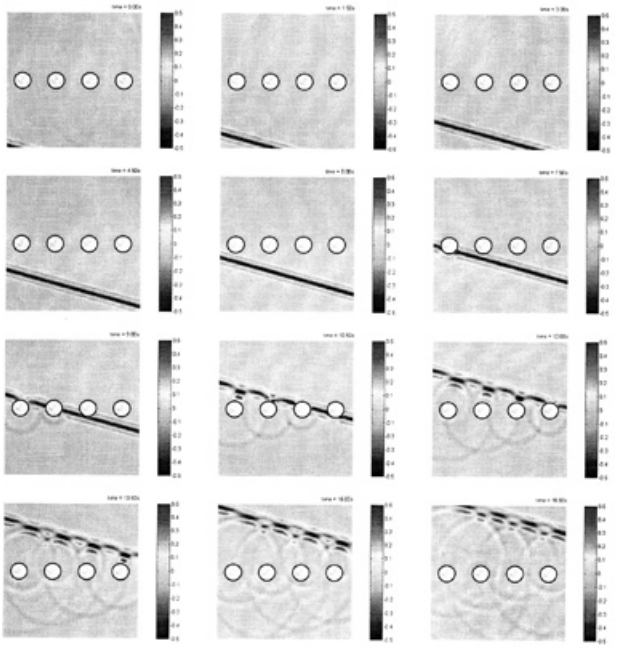

Fig.17. Snapshots of the displacement field for the model given in Fig. 9(b) (four elastic inclusions). Twelve times are depicted from t_i = 0.0s to t_i = 16.5s. The observation area is defined by -8a≤ x≤8a and -8a≤ y≤8a. Excitation given by oblique incidence of anti-plane S-wave ψ = 75° and a Ricker wavelet of t_p = 1.0s.

Conclusions

We have studied an analytic solution to compute the transient response and multiple scattering by a linear array of empty, elastic, and rigid cylinders. The formulation is two-dimensional and is constructed by the superposition of the incident field and the waves diffracted by each obstacle. Here, the incident wave field is given by an anti-plane S-wave. The new interpretation of results and relevant examples were discussed. The normalized displacement amplitude relative to the incident field versus distance was plotted for specific frequencies. It was possible to identify the wave propagation behavior by means of computed synthetic seismograms and snapshots. It is shown that a conspicuous attenuation effect is observed by the array. A double response is produced by the presence of the elastic obstacles: reductions at the incidence side and amplifications at the opposite side, rather than the rigid cylinders, where the inverse response was identified.

The results reported here allow us to aim new paths of research and practical ways to describe and analyze the seismic response and multiple scattering in heterogeneous media. The analytical formulation reviewed in this paper offers a relatively simple way, with low computation cost, to understand the diffraction and multiple scattering of elastic waves by linear array of regularly distributed obstacles. The advantages and limitations of these techniques give us a complementary view of a not widely explored field of research. We are interested in the close future to develop these analytical formulations for several scatterers in arbitrary or randomly distributed configurations. The treatment of vector problem is been reviewed and constitutes the second part of this work. It is obvious that the 3D problem is extremely expensive in CPU and more, if the numerical computations do not take advantage of the mathematical properties of models. The most popular methods (finite differences, finite elements and spectral methods) are commonly used due to their easy implementation and programming. The 2D analytic formulation presented here appears to be a very low demand computational technique that only requires a good mathematical treatment and a PC. The applications of the numerical and analytical solutions for 3D multiple scattering problems are still open and offer a wide research area in several fields of science and engineering. The solution for 2 and 3D problems are now available using super computers or clusters and it is possible to carry on with complicated models. However, the characterization and the fundamental comprehension of the simplest parameters in a realistic model require more versatile mathematical formulations.

Acknowledgements

We wish to thank Jim Spurlin for his valuable suggestions to this work and Sergio Chávez-Pérez for his critical reading. To Dimitri Komatitsch for previous comparisons and computations of some results. This work was partly supported by Instituto Mexicano del Petróleo through The Naturally Fractured Reservoir Program, under Grant D01341, and the Exploration Technologies Research Program, by CONACYT ,under grant NC-204, and Instituto de Ingeniería, UNAM.

Appendix. Graf´s Addition Theorem

In this paper, Graf´s addition theorem is used to represent the scattered waves by the j-th cylinder in terms of the coordinate system l as follows:

$$H_m^{(2)}(kr_j)\begin{matrix}\cos n\theta_j \\ \sin n\theta_j\end{matrix} = \frac{1}{2}\sum_{m=0}^{\infty}(-1)^m \varepsilon_m J_m(kr_l)\begin{matrix}K_m^n(kd_{jl})\cos m\theta_l \\ L_m^n(kd_{jl})\sin m\theta_l\end{matrix} \qquad (15)$$

for j < l, or

$$H_m^{(2)}(kr_j)\begin{matrix}\cos n\theta_j \\ \sin n\theta_j\end{matrix} = \frac{1}{2}(-1)^n\sum_{m=0}^{\infty}\varepsilon_m J_m(kr_l)\begin{matrix}K_m^n(kd_{jl})\cos m\theta_l \\ L_m^n(kd_{jl})\sin m\theta_l\end{matrix} \qquad (16)$$

if j > l.

Bibliography

Abramowitz, M., and I. A. Stegun. Handbook of Mathematical Functions with Formulas, Graphs and Mathematical Tables (National Bureau of Standards, Applied Mathematics Series 55, Washington 1964).

Ávila-Carrera, R., and F. J. Sánchez-Sesma, 2006. Scattering and Diffraction of Elastic P- and S-waves by a Spherical Obstacle: A Review of the Classical Solution. Geof. Inter., 45, 3-21.

Avilés, J. and F. J. Sánchez-Sesma, 1983. Piles as Barriers for Elastic Waves, J. Geotech. Engn., 109, 1133-1146.

Benites, R., K. Aki and K. Yomogida, 1992. Multiple Scattering of SH Waves in 2-D Media with Many Cavities, Pure Appl. Geophys., 133, 353-390.

Davis, C. A., V. W. Lee and J. P. Bardet, 2001. Transverse Response of Underground Cavities and Pipes to

Incident SV Waves, Earth. Engn. Struc. Dyn. 30, 383-410.

Foldy, L. 1945. The Multiple Scattering of Waves: 1. General Theory of Isotropic Scattering by Randomly Distributed Scatterers, Phys. Rev. 67, 107-119.

Frisch, U. Wave Propagation in Random Media (Academic press, New York, 1968).

Gritto, R., V. A. Korneev and L. R. Johnson, 1995. Low Frequency Elastic Wave Scattering by an Inclusion: Limits of Applications, Geophys. J. Inter. 120, 677-692.

Gritto, R., V. A. Korneev and L. R. Johnson, 1999. Nonlinear Three-dimensional Inversion of Low Frequency Scattered Elastic Waves, Pure Appl. Geophys. 156, 557-589.

Ishimaru, A. Wave Propagation and Scattering in Random Media (Oxford University Press 1997).

Kanaun, S. K., V. M. Levin and F. J. Sabina, 2004. Propagation of Elastic Waves in Composites with Random Set of Spherical Inclusions (Effective Medium Approach), Wave Motion, 40, 69-88.

Kikuchi, M. 1981. Dispersion and Attenuation of Elastic Waves Due to Multiple Scattering from Inclusions, Phys. Earth Planet. Inter. 25, 159-162.

Lax, M. 1951. Multiple Scattering of Waves, Rev. Mod. Phys. 23, 287-310.

Mow, C. C. and Y. H. Pao. The Diffraction of Elastic Waves and Dynamic Stress Concentrations (A reported prepared for United States Air Force Project Rand 1971).

Sheng, P. Introduction to Wave Scattering, Localization and Mesoscopic Phenomena (Academic Press, New York 1995).

Tsang, L., J. A. Kong and K. H. Ding. Scattering of Electromagnetic Waves Vol. 1; Theory and Applications (Wiley Interscience 2000).

Twersky, V. 1952. Multiple Scattering of Radiation by an Arbitrary Planar Configuration of Parallel Cylinders and by Two Parallel Cylinders, J. Appl. Phys. 23, 407-414.

Varadan, V. K., V. V. Varadan and Y. H. Pao, 1978. Multiple Scattering of Elastic Waves by Cylinders of Arbitrary Cross Section 1. SH waves, J. Acoust. Soc. Am. 63, 1310-1319.

Varadan, V. K. and V. V. Varadan. Acoustic, Electromagnetic and Elastic Wave Scattering: Focused on the T-Matrix Approach (Pergamon, New York 1980).

Veksler, N. D., A. Lavie and B. Dubus, 2000. Peripheral Waves Generated in a Cylindrical Shell with Hemispherical end Caps by a Plane Acoustic Wave at Axial Incidence, Wave Motion, 4, 349-369.

Vlastos, S., E. Liu, I. G. Main and X. Y. Li, 2003. Numerical Simulation of Wave Propagation in Media with Discrete Distributions of Fractures: Effects of Fracture Sizes and Spatial Distributions, Geophys. J. Inter. 152, 649-668.

Waterman, P. C. and R. Truell, 1961. Multiple Scattering of Waves, J. Math. Phys. 2, 512-537.

Yin-bin, L., W. Ru-Shan and C. F. Ying, 2000. Scattering of Elastic Waves by an Elastic or Viscoelastic Cylinder, Geophys. J. Inter. 142, 439-460.

R. Ávila-Carrera[1]*, F. J. Sánchez-Sesma[2] and J. Avilés[3]
[1]*Instituto Mexicano del Petróleo*
Eje Central Lázaro Cárdenas 152; Mexico, City, Mexico.
[2]*Instituto de Ingeniería, Universidad Nacional Autónoma de México. Mexico City, Mexico*
[3]*Instituto Mexicano de Tecnología del Agua; Paseo Cuauhnáhuac 8532; Jiutepec, Morelos. México.*
**Corresponding author: rcarrer@imp.mx*